Supplementary information
for

Dual H-bond activation of NHC-Au(I)-Cl complexes with amide functionalized side-arms assisted by H-bond donor substrates or acid additives

Otto Seppänen,[a#] Santeri Aikonen,[a#] Mikko Muuronen,[a†] Carla Alamillo-Ferrer,[b] Jordi Burés,[b] and Juho Helaja*[a]

a) Department of Chemistry, University of Helsinki, A. I. Virtasen aukio 1, P.O. Box 55, 000014, Helsinki (Finland). Email: juho.helaja@helsinki.fi

b) The University of Manchester, School of Chemistry, Oxford Road, M13 9PL Manchester, U.K.

 # The authors have equal contribution

† Current affiliation: BASF SE, Carl-Bosch-Str. 38, 67056 Ludwigshafen, Germany.

Table of Contents

S1 Computational details

Density functional theory (DFT) level computations were carried out with TURBOMOLE 7.3[1] and ORCA 4.1[2] program packages. Both TURBOMOLE and ORCA were used for searching transition states, whereas geometries, vibrational frequencies, and single-point energies were computed with TURBOMOLE. Lowest energy conformers were searched with CREST[3] and GFN-xTB.[4] A dispersion corrected mGGA functional TPSS-D3,[5,6] was used for the structure optimisation with def2-TZVP[7] basis sets. Final single-point energies were calculated using the PW6B95-D3[8] hybrid functional and def2-TZVPD basis sets.[9] These functionals were chosen because they provide accurate geometries and energies for wide range of systems.[10] The multipole accelerated resolution-of-identity approximation for Coulomb term[11,12] was used with TURBOMOLE with the corresponding auxiliary basis sets.[13] The grid *m4* and default convergence criteria of 10^{-7} and 10^{-6} were used for density and energy, respectively. The 3D images were created using CYLview.[14]

Solvation effects were accounted in all structure optimizations using the COSMO[15] solvation model with dielectric constant of dichloromethane (DCM, 8.9), and in final energies COSMO-RS solvation model was used as implemented in COSMOtherm19 program package[16] with BP_TZVPD_FINE_19.ctd parameter file based on BP86[17]/def2-TZVPD computational level. The Gibbs free energies in solution were calculated according to published protocol: $G = E_{gas}(SCF)$ + chem.pot. + G_{solv},[18] where $E_{gas}(SCF)$ is the final energy of the system in gas phase at PW6B95-D3/def2-TZVPD level, chem.pot. is the chemical potential calculated at the optimisation level (TPSS-D3/def2-TZVP) using the qRRHO approximation by Grimme,[19] and G_{solv} is the solvation free energy of each species in DCM from COSMO-RS. All thermodynamic functions were calculated at 298.15 K and vibrational frequencies were used without scaling. The reference state for Gibbs free energies at room temperature is 1 bar of ideal gas and 1 mol of liquid solvent.

The pK_a values were calculated according to Eq. 1

$$pK_a = \frac{\Delta G}{RTln(10)} \approx \frac{\Delta G}{1.364} \qquad \text{Eq. 1}$$

Where ΔG is the acid dissociation free energy: HA → H^+ + A^-, R is the gas constant and T is temperature in Kelvins. The proton's solvation free energy of -207.7 kcal/mol in DCE[20] was used to balance the acid dissociation.

The gold-affinities for different conjugate bases of strong acids presented in Table 2 in the main body were calculated relative to the Au-Cl bond strength as is shown in Figure S1.

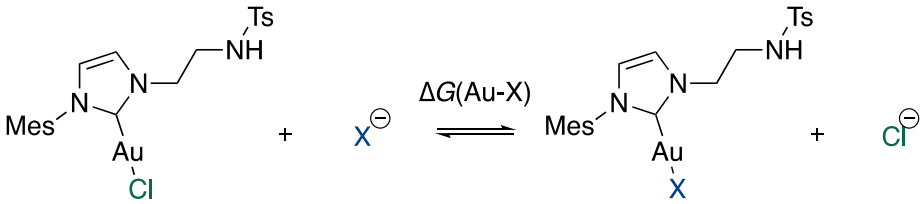

Figure S1. Equilibrium used to calculate the Au-X bond strength.

S2 Reaction free energy profiles

The effect of water assisted (see Figure S2) and substrate assisted (see Figure S3) chloride solvation was compared in addition to chloride staying close to the active centre in Figure S4. It is generally agreed that the protodeauration is the rate-determining step (RDS), but however, for oxazoline cyclisation,[21,22] the rate of the reaction is highly dependent on the ligand/counterion combination.[23] The computational mechanism study for Au(III) catalysed oxazoline synthesis[24] demonstrated that both substrate and the product can mediate the proton transfer, while product is the more efficient agent for proton transfer. Thus, we compare the energetics with product as the agent in proton transfer in the absence of chloride with the free energies for chloride-assisted protodeauration.

The activation free energy barrier of the RDS **TS3-Cl**$^{-}$ is higher if additional substrate coordinates chloride out of the system (Figure S3) whereas water assisted solvation of the chloride (Figure S2) favours the **TS3-Cl**$^{-}$ over **TS3**. In the **TS3** the chloride assists in the cyclisation by coordination (Figure S4). However, in the first step of the protodeauration, **TS4** and **TS4-Cl**$^{-}$, the latter is lower in energy for both water and substrate assisted chloride abstraction as the bidentate (monodentate) H-bonding between NHs and chloride is disrupted by **4a**, see Figure S2, Figure S3, and Figure S4. Same trend is observed in the second step of protodeauration, **TS5** and **TS5-Cl**$^{-}$, as the chloride mediated **TS5** is higher in energy than the product mediated **TS5-Cl**$^{-}$, see Figure S2, Figure S3, and Figure S4.

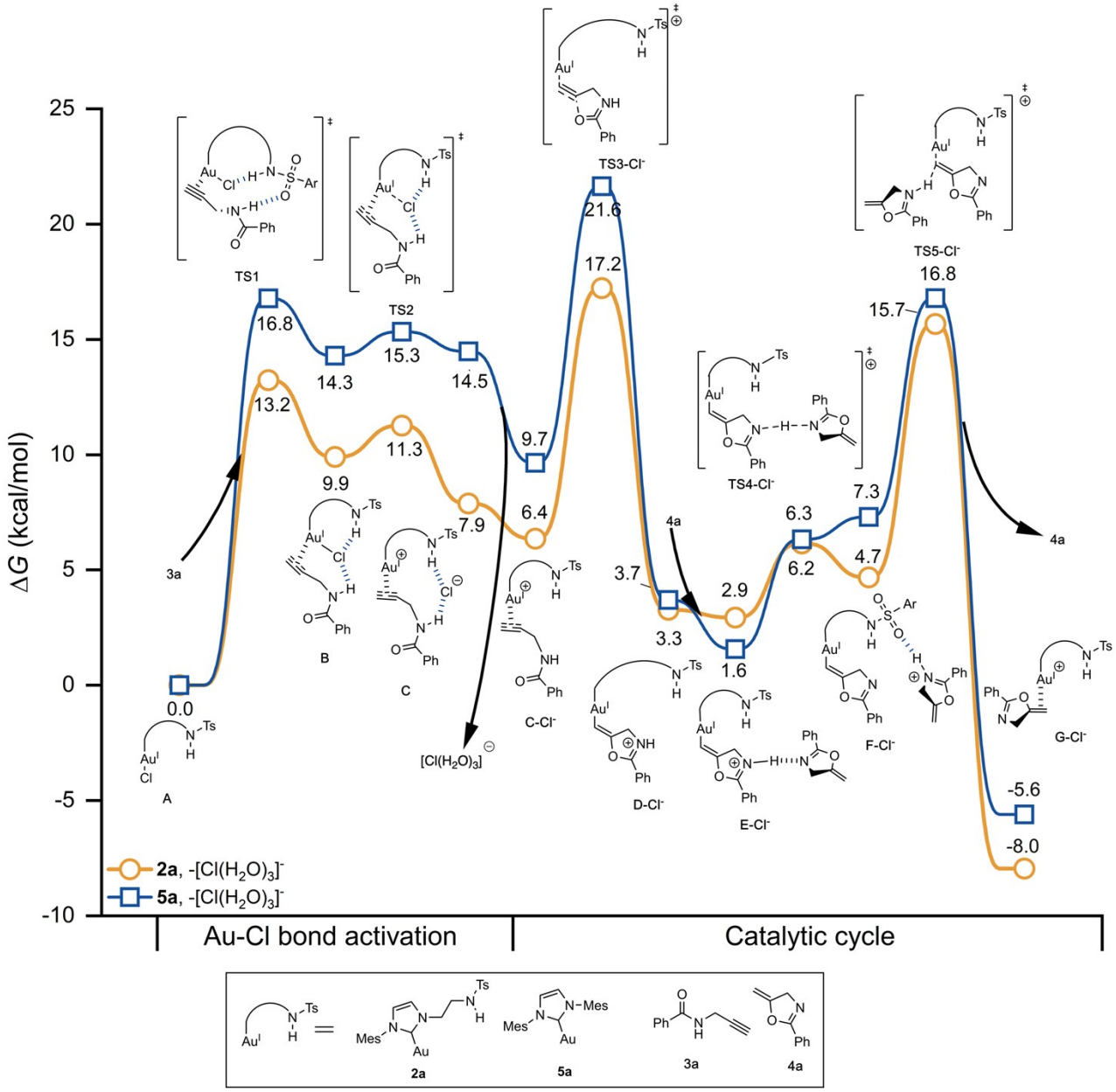

Figure S2. The Gibbs free energy profile for water assisted abstraction of chloride from the catalyst centre. Structures with **5a** are similar to the schematic drawings but without the side arm.

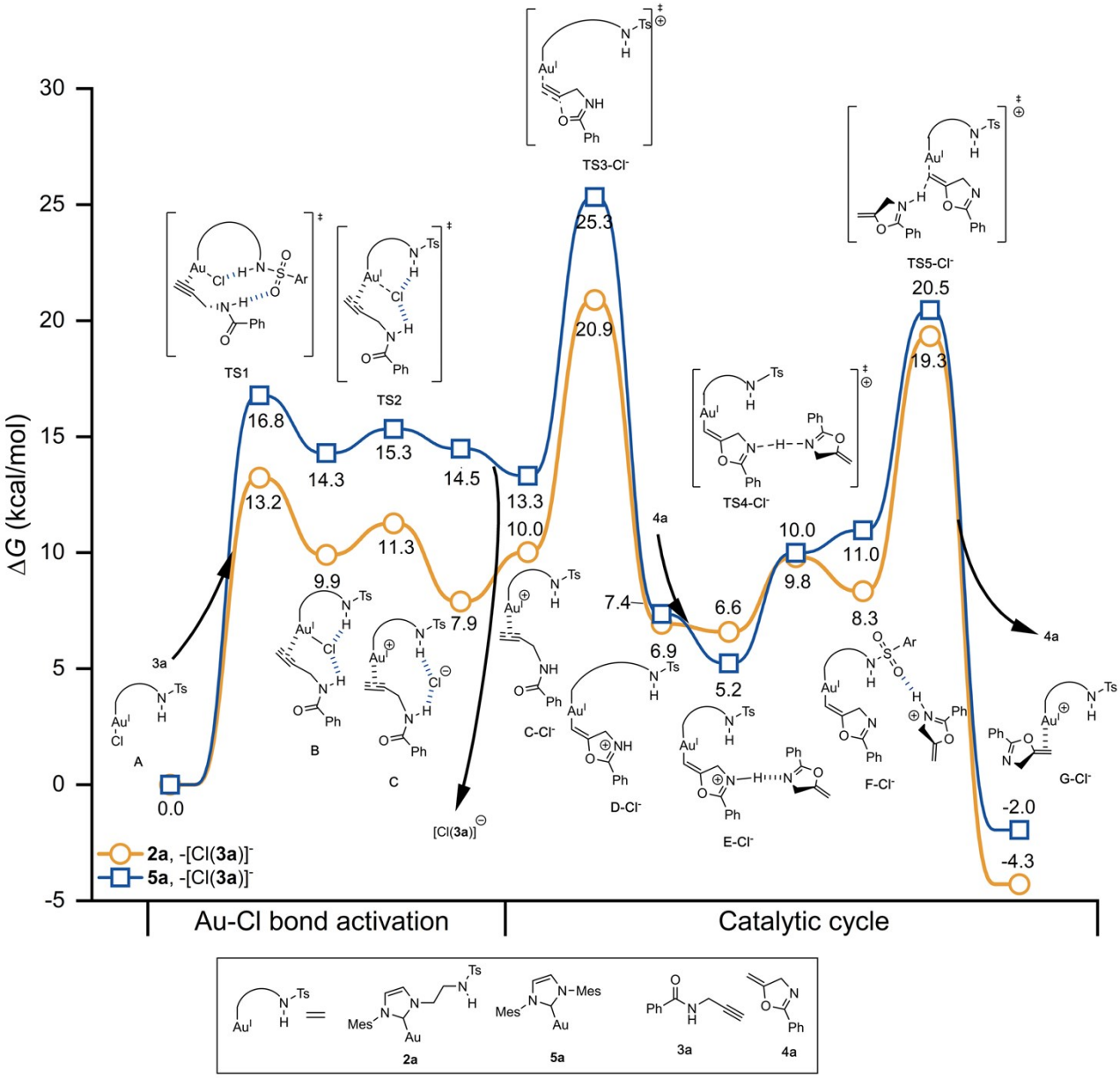

Figure S3. The Gibbs free energy profile for substrate assisted abstraction of chloride from the catalyst center. Structures with **5a** are similar to the schematic drawings but without the side arm.

Protodeauration, **TS5** in Figure S4, is the RDS in the **2a** catalysed reaction as the activation free energy barrier is 21.3 kcal/mol. With the catalyst **5a** the *5-exo-dig* cyclisation is the RDS with 23.2 kcal/mol activation free energy and the protodeauration is of similar magnitude with **2a**: 21.6 kcal/mol.

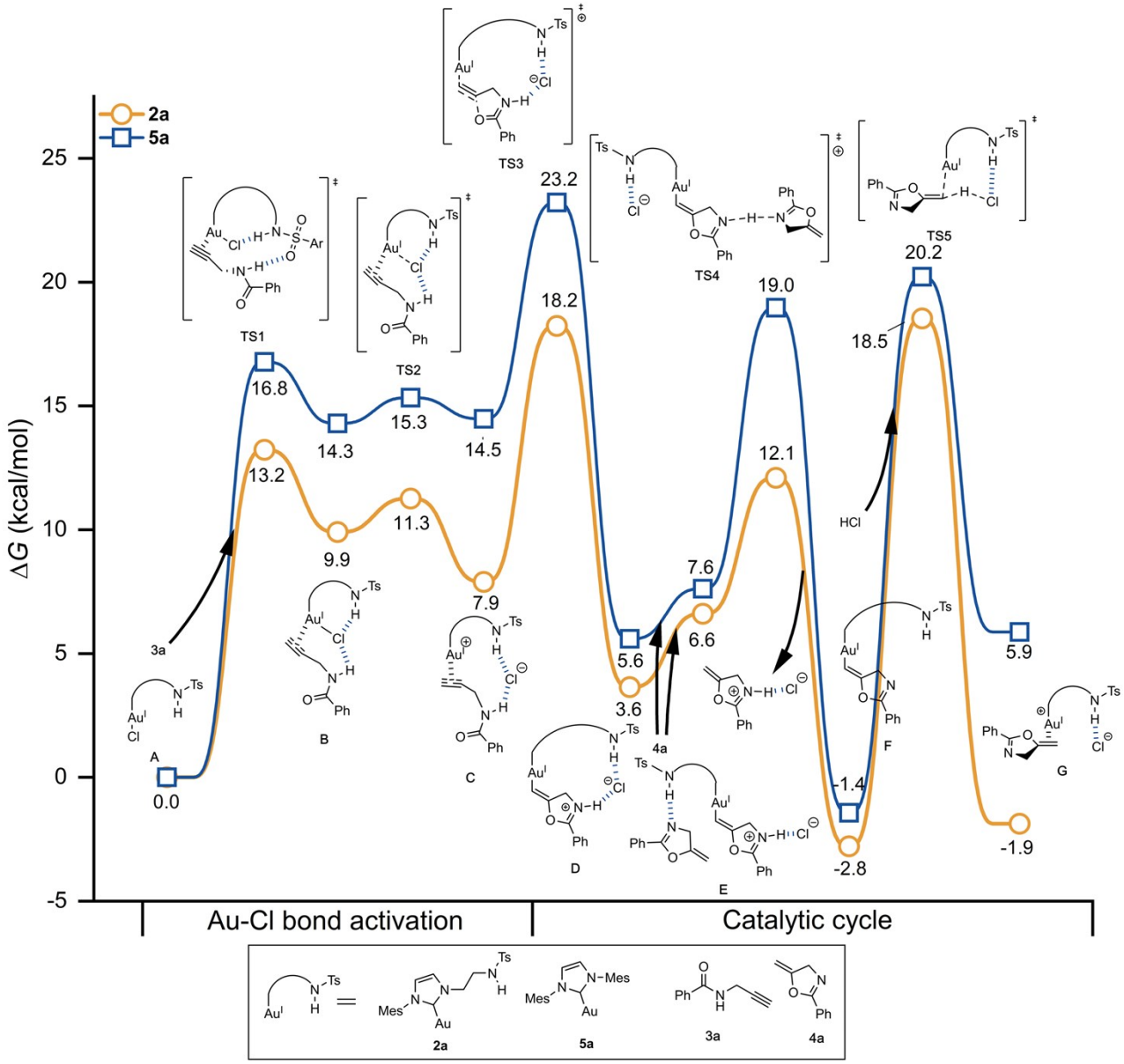

Figure S4. Gibbs free energy profiles when chloride coordinated by HB donor(s) near the catalytic center. Structures with **5a** are similar to the schematic drawings but without the side arm.

S3 Images of selected structures

In **2a-TS1** the substrate's NH is hydrogen bonded to side-arm's sulfonyl oxygen, and side-arm's NH is hydrogen bonded to the chloride, see Figure S5. If the substrate's NH is also coordinated to the chloride (**2a-TS1'**), the activation free energy barrier is 0.8 kcal/mol higher, whereas if the substrate's NH does not form HB the activation free energy barrier is 5.0 kcal/mol higher (**2a-TS1''**). For comparison, monodentate HB to chloride in **5a-TS1** has 3.6 kcal/mol higher activation free energy barrier compared to **2a-TS1**. In **2a-TS1** the Au-Cl and $C_{terminal}$-Au bond lengths are 2.52 Å and 2.41 Å, respectively, while in **5a-TS1** the bond lengths are 2.57 Å and 2.77 Å, respectively. Importantly, in all **2a**'s **TS1**s the alkyne's terminal hydrogen is pointing to the mesityl ring that might inhibit the reactivity of internal alkynes due to steric hindrance.

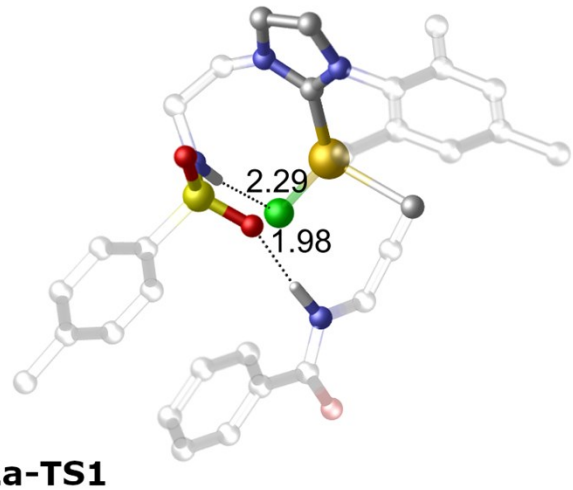

2a-TS1
$\Delta G^{\ddagger}$ = 13.2 kcal/mol

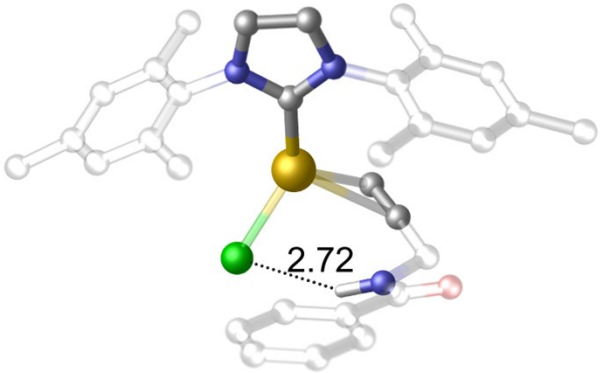

5a-TS1
$\Delta G^{\ddagger}$ = 16.8 kcal/mol

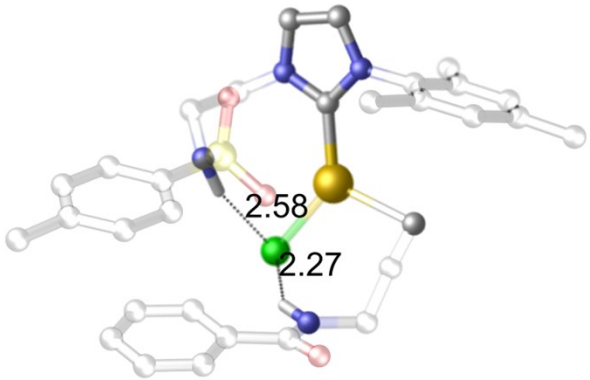

2a-TS1'
$\Delta G^{\ddagger}$ = 14.0 kcal/mol

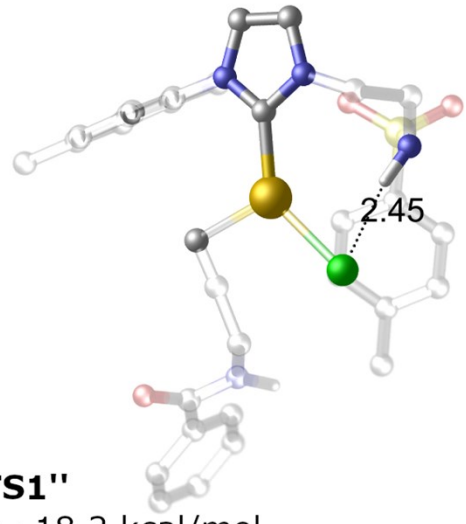

2a-TS1''
$\Delta G^{\ddagger}$ = 18.2 kcal/mol

Figure S5. The **TS1** structures for **2a** and **5a**.

The bidentate HB stabilises the **2a-B** by 4.4 kcal/mol compared to monodentate H-bonding in **5a-B**, see Figure S6. The Au-Cl bond length is elongated from 2.31 Å to 2.58 Å in both **2a** and **5a**. The bond angle C_{NHC}-Au-Cl decreases from 179.8° to 105.0° and from 179.9° to 96.2° with **2a** and **5a**, respectively. The $C_{terminal}$-Au bond lengths are 2.12 Å in both **2a** and **5a** while the C_{NHC}-Au-$C_{terminal}$ bond angles are 121.5° and 129.6° for **2a** and **5a**, respectively.

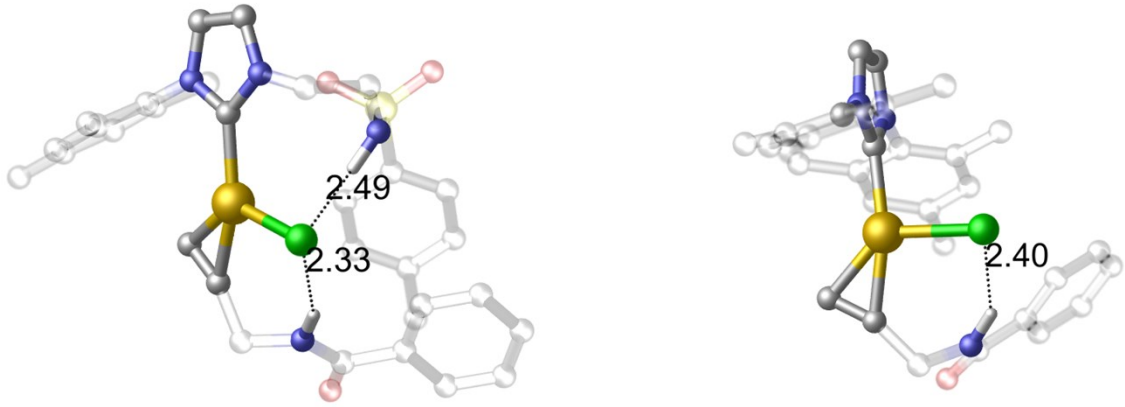

2a-B
ΔG = 9.9 kcal/mol

5a-B
ΔG = 14.3 kcal/mol

Figure S6. The **B** structures for **2a** and **5a**.

In **TS2** the hydrogen bond distances between the NHs and chloride decrease by 0.22 Å on average and the bidentate HB with **2a** lowers the activation free energy barrier by 4.0 kcal/mol compared to **5a**, see Figure S7. The Au-Cl and $C_{terminal}$-Au bond lengths for **2a** are 2.93 Å and 2.16 Å, respectively, while for **5a** the bond lengths are 3.03 Å and 2.17 Å, respectively.

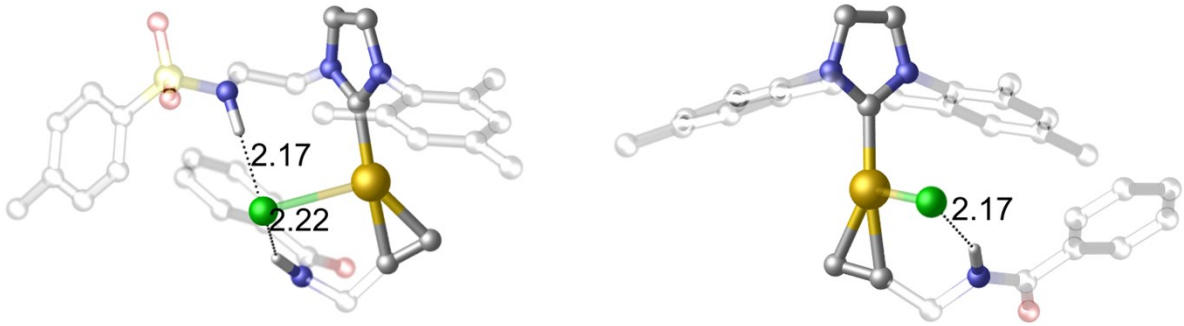

2a-TS2
$\Delta G^{\ddagger}$ = 11.3 kcal/mol

5a-TS2
$\Delta G^{\ddagger}$ = 15.3 kcal/mol

Figure S7. The **TS2** structures for **2a** and **5a**.

In the **C** intermediates the distance between Au and chloride is 3.93 Å and 3.18 Å for **2a** and **5a**, respectively. With **2a** the chloride is hydrogen bonded to both NHs and with **5a** to the substrate.

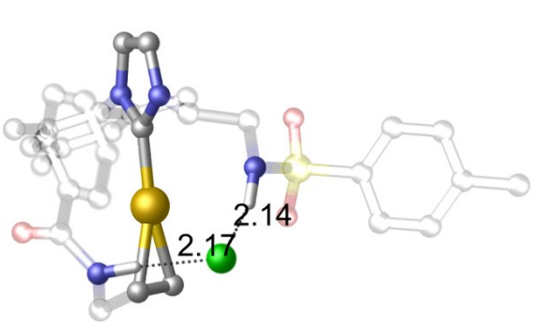

2a-C
ΔG = 7.9 kcal/mol

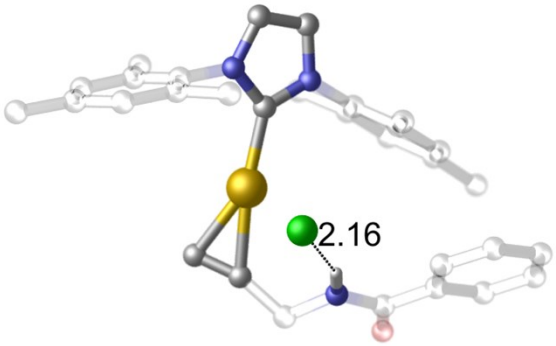

5a-C
ΔG = 14.5 kcal/mol

Figure S8. The **C** structures for **2a** and **5a**.

The side-arm of **2a** assists in the *5-exo-dig* cyclisation step by hydrogen bonding either with the chloride anion or with the substrate's NH, see Figure S9. The hydrogen bonding interactions lower the activation free energy barrier by 5.0 kcal/mol (**TS3**) and by 4.4 kcal/mol (**TS3-Cl**$^-$) compared to **5a**.

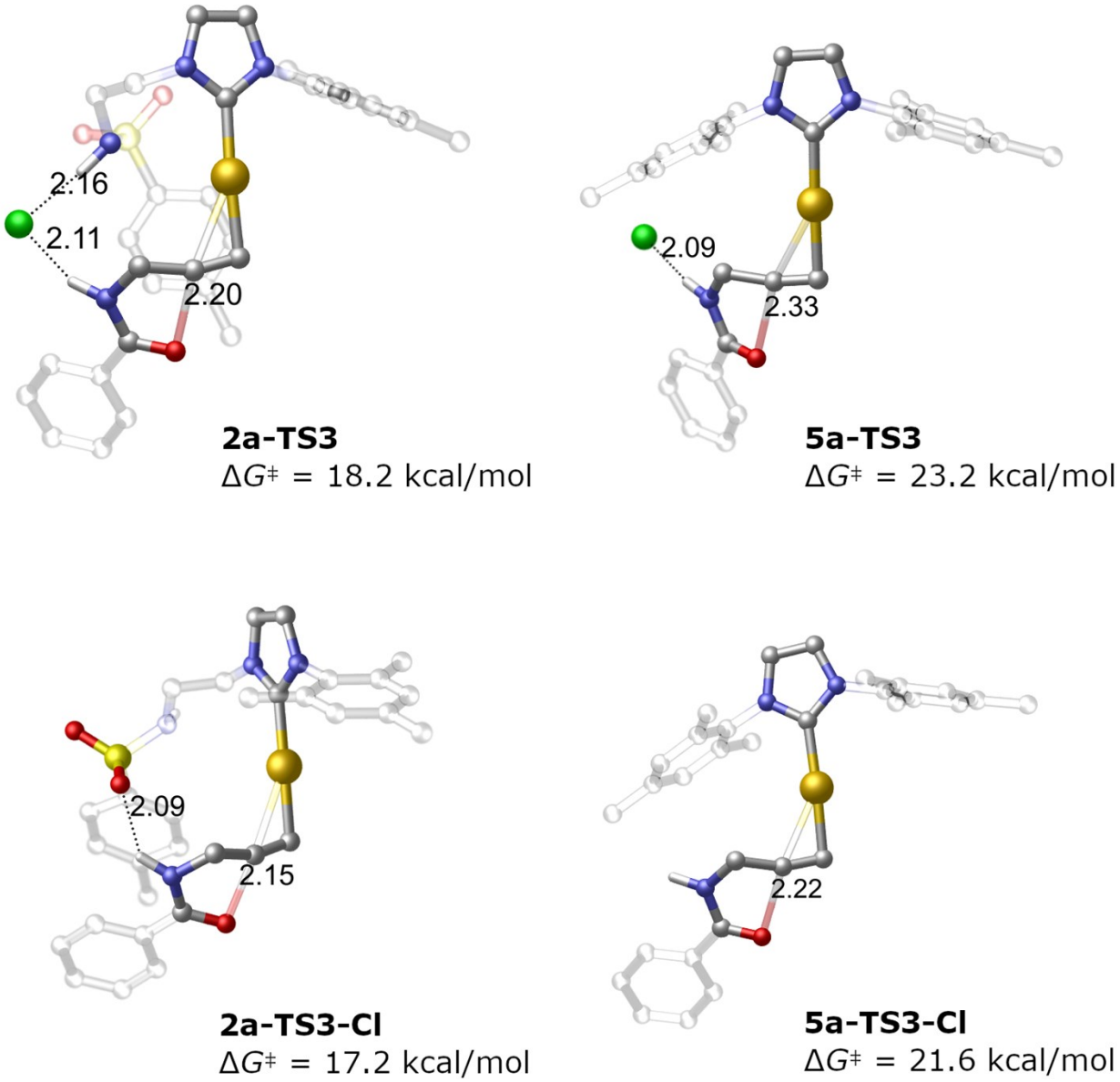

Figure S9. The cyclisation transition states **TS3** (top row) and **TS3-Cl**$^-$ (bottom row) for **2a** (left column) and **5a** (right column). The **2a-TS3-Cl** and **5a-TS3-Cl** free energies are with water solvated chloride ion.

References

[1] F. Furche, R. Ahlrichs, C. Hättig, W. Klopper, M. Sierka, F. Weigend, *WIREs Comput. Mol. Sci.*, 2014, **4**, 91–100.
[2] F. Neese, *WIREs. Comput. Mol. Sci*., 2017, **8**, e1327.
[3] P. Pracht, F. Bohle, S. Grimme. *Phys. Chem. Chem. Phys.*, 2020, **22**, 7169–7192.
[4] a) S. Grimme, C. Bannwarth, P. Shushkov, *J. Comput. Theory Chem.*, 2017, **13**, 1989–2009; b) C. Bannwarth, S. Ehlert, S. Grimme, *J. Comput. Theory Chem.*, 2019, **15**, 1652–1671.
[5] J. Tao, J. P. Perdew, V. N. Staroverov, G. E. Scuseria, *Phys. Rev. Lett.* 2003, **91**, 146401.
[6] S. Grimme, J. Antony, S. Ehrlich, H. Krieg, *J. Chem. Phys.*, 2010, **132**, 154104.
[7] F. Weigend, R. Ahlrichs, *Phys. Chem. Chem. Phys*., 2005, **7**, 3297-3305.
[8] Y. Zhao, D. G. Truhlar, *J. Phys. Chem. A*, 2005, **109**, 5656–5667.
[9] D. Rappoport, F. Furche, *J. Chem. Phys.*, 2010, **133**, 134105
[10] a) L. Goerigk and S. Grimme, *Phys. Chem. Chem. Phys.*, 2011, **13**, 6670–6688; b) L. Goerigk, A. Hansen, C. Bauer, S. Ehrlich, A. Najibi and S. Grimme, *Phys. Chem. Chem. Phys.*, 2017, **19**, 32184–32215; M. Bühl, C. Reimann, D. A. Pantazis, T. Bredow and F. Neese, *J. Chem. Theory Comp.*, 2008, **4**, 1449–1459.
[11] M. Sierka, A. Hogekamp, R. Ahlrichs, *J. Chem. Phys.*, 2003, **118**, 9136–9148.
[12] K. Eichkorn, O. Treutler, H. Öhm, M. Häser, R. Ahlrichs, *Chem. Phys. Lett.*, 1995, **240**, 283–290.
[13] F. Weigend, Phys. *Chem. Chem. Phys.*, 2006, **8**, 1057–1065.
[14] C. Y. Legault, CYLview, 1.0b; Université de Sherbrooke, 2009 (http://www.cylview.org)
[15] A. Schäfer, A. Klamt, D. Sattel, J. C. W. Lohrenz, F. Eckert, *Phys. Chem. Chem. Phys*., 2000, **2**, 2187-2193.
[16] a) COSMO*therm*, Version C3.0, Release 19.01; COSMOlogic GmbH & Co. KG, http://www.cosmologic.de b) F. Eckert, A. Klamt, *AIChE Journal*, 2002, **48**, 369; c) A. Klamt, V. Jonas, T. Bürger, J. C. Lohrenz, *J. Phys. Chem. A*, 1998, **102**, 5074. d) A. Klamt, *J. Phys. Chem.*, 1995, **99**, 2224.
[17] a) A. D. Becke, *Phys. Rev. A*, 1988, **38**, 3098; b) J. P. Perdew, *Phys. Rev. B*, 1986, **33**, 8822.
[18] A. Hellweg, F. Eckert, *AIChE J.*, 2017, **63**, 3944-3954.
[19] S. Grimme, *Chem. Eur. J.*, 2012, **18**, 9955 – 9964. Authors also thank Prof. S. Grimme for providing the thermo-program for using the quasi-RRHO.
[20] E. Paenurk, K. Kaupmees, D. Himmel, A. Kütt, I. Kaljurand, I. A. Koppel, I. Krossing, I. Leito, *Chem. Sci.*, 2017, **8**, 6964-6973.
[21] W. Wang, G. B. Hammond and B. Xu, *J. Am. Chem. Soc.,* 2012, **134**, 5697-5705.
[22] a) A. S. K. Hashmi, A. M. Schuster and F. Rominger, *Angew. Chem. Int. Ed*., 2009, **48**, 8247-8249; b) A. S. K. Hashmi, *Pure Appl. Chem.*, 2010, **82**, 657-668; c) J. P. Weyrauch, A. S. K. Hashmi, A. Schuster, T. Hengst, S. Schetter, A. Littmann, M. Rudolph, M. Hamzic, J. Visus, F. Rominger, W. Frey and J. W. Bats, *Chem. Eur. J.*, 2010, **16**, 956-963; d) O. A. Egorova, H. Seo, Y. Kim, D. Moon, Y. M. Rhee and K. H. Ahn, *Angew. Chem. Int. Ed.*, 2011, **50**, 11446-11450.
[23] L. Biasiolo, A. Del Zotto and D. Zuccaccia, *Organometallics*, 2015, **34**, 1759-1765.
[24] Y. Liu, P. Liu, B. Ling, G. Chen, T. Chen, Y. Li, S. Bi and D. Zhang, *Eur. J. Org. Chem.,* 2019, 6822-6829.